



Dynamic response analysis of monorail bridges under moving trains and riding comfort of trains

Lee, Chang Hun

Kim, Chul Woo

Kawatani, Mitsuo

Nishimura, Nobuo

Kamizono, Takumi

(Citation)

Engineering Structures, 27(14):1999-2013

(Issue Date)

2005-12

(Resource Type)

journal article

(Version)

Accepted Manuscript

(URL)

<https://hdl.handle.net/20.500.14094/90000159>



Dynamic Response Analysis of Monorail Bridges under Moving Trains and Riding Comfort of Trains

Chang Hun Lee¹, Chul Woo Kim², Mitsuo Kawatani^{*2},

Nobuo Nishimura¹ and Takumi Kamizono²

¹*Dept. of Civil Eng., Osaka University, 2-1 Yamadaoka, Suita, Osaka 565-0871, Japan*

²*Dept. of Civil Eng., Kobe University, 1-1 Rokkodai, Nada, Kobe 657-8501, Japan*

ABSTRACT

This paper introduces an analytical procedure to derive equations of motion for the monorail train-bridge interaction based on Lagrange's formulation to investigate riding comfort of moving monorail trains on bridges. A 15DOF dynamic model is assumed for a car in a monorail train that consists of driving, steering, and stabilizing wheels. It is based on the finite element method for modal analysis using three-dimensional models for a monorail bridge. Dynamic behaviors of a rationalized monorail bridge with a simplified structural system are investigated in comparison with those of a conventional monorail bridge using the developed analytical method. Riding comfort of running trains on the rationalized monorail bridge based on ISO2631 is estimated using 1/3 octave band spectral analysis. Observations indicate that a rational type bridge does not engender difficulties related to the riding comfort of the monorail train, even when considering the longest traveling time of passengers between terminals.

Keywords: Monorail bridge; Bridge-train interaction; Dynamic response analysis; 15DOFs of train model

1. Introduction

Traffic problems in major cities around the world during the last two decades have presented important needs of new transportation systems. Consequently, the challenge to adopt new transportation modes has yielded monorail systems. Monorail trains' weight on a bridge reaches up to 50% of the weight of a couple of track girders. Another interesting feature is in the straddle-type monorail: the bogie system comprises steering and stabilizing wheels that firmly grasp the track girder (see Fig. 1) to increase running stability.

Modern bridge design requires not only strength, but also cost-efficiency. That situation

* Corresponding author. Phone: +81-78-803-6278; Fax: +81-78-803-6069. E-mail address: m-kawa@kobe-u.ac.jp

stimulates structural engineers to create a concept of rationalized design strategy even for a monorail bridge. Therefore, a new type of rationalized steel-concrete composite bridge for monorails has been developed in Japan. The rationalized monorail bridge adopts a simplified lateral bracing system. The RC track girder is another advanced concept to enhance braking performance of monorail trains. Advantages of such a simplified structural system of monorail bridges include the simplicity in relation to a life-cycle cost. However, the simplified lateral bracing system of the rationalized monorail bridge may engender problems related to vibration serviceability, especially in a lateral direction, as a consequence of moving trains, earthquakes, winds, etc. [1].

Some studies [2–11] have investigated vibration in railway and highway bridges under moving trains and other vehicles. As for long-span bridge-train systems, Diana and Cheli [2] pointed out two fundamental aspects to be investigated: one is the bridge safety that is attributable to train passage; the other is the trains' running characteristics including passenger comfort. Au *et al.* [5] described a study of impact effects on a cable-stayed bridge under railway train loading. Lei and Noda [6] studied dynamic responses of the vehicle and track coupling system with random railway line irregularity. Ju and Lin [7] assessed vibration characteristics of a three-dimensional arch bridge during high-speed train passage. Song *et al.* [8] proposed a new finite element model for three-dimensional FE analysis of high-speed train-bridge interaction, in which various improved finite elements were used for modeling structural constituents of a railway bridge. Kwark *et al.* [9] presented a numerical method showing reasonable results concerning the dynamic behavior analysis of bridges under trains running at high speed. For a highway bridge, Hutton and Cheung [10] studied realistic bridge decks and vehicle parameters for effects of several variables upon the dynamic response of the bridge deck. Kawatani and Kim [11] investigated characteristics of dynamic wheel loads of heavy vehicles running on bridges and rigid surfaces using a three-dimensional analytical model. However, few investigations have addressed riding comfort of monorail trains according to bridges' structural types.

This study is intended to investigate dynamic characteristics of a rationalized monorail bridge through comparison with those of a conventional bridge under moving trains. Riding comfort of monorail trains on a rationalized bridge is another important purpose of this study. The investigations are based on the analytical procedure developed in this study. The validity of developed equations of motion for a monorail train-bridge interaction system was verified through comparison with field-test data [1, 12]. Riding comfort of trains running on a rationalized monorail bridge is estimated using 1/3 octave band spectral analysis based on ISO2631 [13, 14].

2. Analytical procedure of train-monorail structure interaction system

2.1 Monorail train

A monorail train has two bogies on the front and rear axles, respectively. Each bogie has driving wheels, and steering and stabilizing wheels that firmly grasp the track girder (see Fig. 2). Figure 3 shows the idealized train model of a dynamic system with 15-degree-of-freedom (15DOF): m indicates the mass; K , the spring constant; C , the damping coefficient; while Z , Y and θ indicate the vertical, lateral, and rotational displacements, respectively. Bouncing, swaying, pitching, rolling, and yawing motions of the body and each bogie are incorporated into this model. On the other hand, behavior in the longitudinal direction is not considered. The monorail train itself is considered rigid and supported by a set of linear springs and dashpots. It is assumed that wheels and rails maintain constant contact. Tables 1 and 2 summarize notations and properties of the train used in this study, respectively. The dynamic properties are taken from manufacturer's data.

Governing equations of the monorail bridge-train interaction system are derived using Lagrange's equation of motion (see Eq. (1)), which has been a popular method to formulate a dynamic system that provides a method with great power and versatility for formulation of equations of motion for any dynamic system [15, 16].

$$\frac{\partial}{\partial t} \left(\frac{\partial T}{\partial \dot{a}_i} \right) - \frac{\partial T}{\partial a_i} + \frac{\partial U_e}{\partial a_i} + \frac{\partial U_d}{\partial \dot{a}_i} = 0 \quad (1)$$

where, T is kinetic energy, U_e is potential energy, U_d is the dissipation energy due to the damping of the system, and a_i means generalized coordinates.

Equations of kinetic energy, potential energy including strain energy, and dissipation energy by viscous damping of a train system are developed by modification of the energy equation for vehicles on highway bridges [11].

$$T = \frac{1}{2} \left[\sum_{v=1}^{nv} \left\{ m_{v11} \dot{Z}_{v11}^2 + m_{v11} \dot{Y}_{v11}^2 + I_{vy11} \dot{\theta}_{vy11}^2 + I_{vz11} \dot{\theta}_{vz11}^2 \right. \right. \\ \left. \left. + \sum_{i=1}^2 \left(m_{v2i} \dot{Z}_{v2i}^2 + m_{v2i} \dot{Y}_{v2i}^2 + I_{vx2i} \dot{\theta}_{vx2i}^2 + I_{vy2i} \dot{\theta}_{vy2i}^2 + I_{vz2i} \dot{\theta}_{vz2i}^2 \right) \right\} \right] \quad (2)$$

$$U_e = \frac{1}{2} \sum_{v=1}^{nv} \left[\sum_{j=1}^2 \sum_{n=1}^2 \left\{ K_{vi1jn} R_{vi1jn}^2 \delta_{1j} + K_{vi2jn} R_{vi2jn}^2 + K_{vi3jn} R_{vi3jn}^2 + K_{vi4jn} R_{vi4jn}^2 \delta_{1j} \right\} + \sum_{i=1}^2 K_{vi511} R_{vi511}^2 \right] \quad (3)$$

$$U_d = \frac{1}{2} \sum_{v=1}^{nv} \left[\sum_{i=1}^2 \sum_{j=1}^2 \sum_{n=1}^2 \{ C_{vi1jn} \dot{R}_{vi1jn}^2 \delta_{1j} + C_{vi2jn} \dot{R}_{vi2jn}^2 + C_{vi3jn} \dot{R}_{vi3jn}^2 + C_{vi4jn} \dot{R}_{vi4jn}^2 \delta_{1j} \} + \sum_{i=1}^2 C_{vi511} \dot{R}_{vi511}^2 \right] \quad (4)$$

In Eqs. (2), (3) and (4), nv represents the total number of cars in a monorail train; subscript v indicates the number of cars on a bridge; I is the mass moment of inertia; and R_{vimjn} denotes the relative displacement at springs. Subscript i is the index for the axle; subscript j indicates the tire position in one bogie ($i, j=1, 2$ indicating front and rear side, respectively). The index for the left and right sides of a train is n , while δ_{ij} is Kronecker's delta function. Table 1 provides details of notations in Eqs. (2), (3) and (4).

Relative displacements can be described as shown in Eq. (5) to Eq. (9).

$$R_{vi1jn} = Z_{v11} - Z_{v2i} + (-1)^n \theta_{vx11} L_{vy2} - (-1)^n \theta_{vx2i} L_{vy2} - (-1)^i \theta_{vy11} L_{vxi} \quad (5)$$

$$R_{vi2jn} = Z_{v2i} - (-1)^j \theta_{vy2i} L_{vx3} + (-1)^n \theta_{vx2i} L_{vy4} - V_{0i2jn} \quad (6)$$

$$R_{vi3jn} = Y_{v2i} - V_{0i3jn} + (-1)^j \theta_{vz2i} L_{vx4} \quad (7)$$

$$R_{vi4jn} = Y_{v2i} - V_{0i4jn} + \theta_{vx2i} L_{vz3} \quad (8)$$

$$R_{vi5jn} = Y_{v11} - Y_{v2i} - \theta_{vx11} L_{vz1} + (-1)^i \theta_{vz11} L_{vxi} \quad (9)$$

In those equations, V_{0imjn} denotes the relative displacement between bridge displacement and surface roughness at the wheel contact point.

2.2 Bridge system

Finite element method (FEM) is adopted for modal analysis as a tool for idealizing bridges for dynamic response analysis. The consistent mass system and Rayleigh damping [17] are adopted, respectively, to form mass and damping matrices of the bridge model. The bridges are considered as an assemblage of beam elements with six DOFs at each node. Guyan reduction is performed [18] to improve the calculation efficiency. Especially, for the monorail bridge, the vertical and lateral wheel loads of trains and torsional moment due to rolling of the train body affect the dynamic response of the monorail bridge. Therefore displacements in relation to vertical, lateral and torsional directions are considered as the master degree-of-freedom, and other three components are assumed as the slave degree-of-freedom throughout the Guyan reduction.

The equation of forced vibration for a bridge is obtained as

$$\mathbf{M}_b \ddot{\mathbf{w}}_b + \mathbf{C}_b \dot{\mathbf{w}}_b + \mathbf{K}_b \mathbf{w}_b = \mathbf{f}_b \quad (10)$$

where \mathbf{M}_b , \mathbf{C}_b and \mathbf{K}_b denote mass, damping, and stiffness matrices of the bridge system, respectively. An external force vector which cars give to the bridge is denoted as \mathbf{f}_b .

The Rayleigh damping scheme is used to form the damping matrix \mathbf{C}_b as a linear combination of the stiffness and mass matrices. The displacement vector of the bridge is \mathbf{w}_b , which can be expressed in terms of the normal coordinate q_i and the mode vector ϕ_i as defined in Eq. (11); (\cdot) represents the derivative with respect to time.

$$\mathbf{w}_b = \sum_i \phi_i q_i = \Phi \cdot \mathbf{q} \quad (11)$$

In that equation, Φ denotes the mode matrix, and \mathbf{q} is the generalized coordinate vector.

The load vector that is attributable to moving monorail trains is given as Eq. (12).

$$\mathbf{f}_b = \sum_{v=1}^{nv} \sum_{i=1}^2 \sum_{m=1}^5 \sum_{j=1}^2 \sum_{n=1}^2 \Psi_{vimjn}(t) \mathbf{P}_{vimjn}(t) \quad (12)$$

Therein, Ψ_{vimjn} is the distribution vector of the wheel loads delivered to each node of the element; \mathbf{P}_{vimjn} is the monorail train wheel load, which can be expressed as the following.

$$\begin{aligned} P_{vi2jn} &= \frac{g}{4} \{m_{v11}(1 - L_{vxi}/L_{vx}) + m_{v2i}\} + K_{vi2jn} R_{vi2jn} + C_{vi2jn} \dot{R}_{vi2jn} \quad ; \quad \text{driving wheel} \\ P_{vi3jn} &= K_{vi3jn} R_{vi3jn} + C_{vi3jn} \dot{R}_{vi3jn} \quad ; \quad \text{steering wheel} \\ P_{vi4jn} &= K_{vi41n} R_{vi41n} + C_{vi41n} \dot{R}_{vi41n} \quad ; \quad \text{stabilizing wheel} \end{aligned} \quad (13)$$

2.3 Dynamic equations of monorail structure-train interaction system

The combination of the interaction force and wheel load at the contact point suggests the following equation of forced vibration for a monorail train-bridge interaction system:

$$\begin{bmatrix} \bar{\mathbf{M}}_b & 0 \\ \text{Symm.} & \mathbf{M}_v \end{bmatrix} \begin{Bmatrix} \ddot{\mathbf{q}} \\ \ddot{\mathbf{A}} \end{Bmatrix} + \begin{bmatrix} \bar{\mathbf{C}}_b^* & \bar{\mathbf{C}}_{bv} \\ \text{Symm.} & \mathbf{C}_v \end{bmatrix} \begin{Bmatrix} \dot{\mathbf{q}} \\ \dot{\mathbf{A}} \end{Bmatrix} + \begin{bmatrix} \bar{\mathbf{K}}_b^* & \bar{\mathbf{K}}_{bv} \\ \text{Symm.} & \mathbf{K}_v \end{bmatrix} \begin{Bmatrix} \mathbf{q} \\ \mathbf{A} \end{Bmatrix} = \begin{Bmatrix} \bar{\mathbf{f}}_b \\ \mathbf{f}_v \end{Bmatrix} \quad (14)$$

where \mathbf{M} , \mathbf{C} and \mathbf{K} indicate the mass, damping, and stiffness matrices, respectively. The force vector is \mathbf{f} . Subscripts b , v and bv denote the bridge, vehicle, and the bridge-vehicle interaction system, respectively. $\bar{\mathbf{M}}_b = \Phi^T \mathbf{M}_b \Phi$; $\bar{\mathbf{C}}_b^* = \Phi^T \mathbf{C}_b \Phi$; $\bar{\mathbf{K}}_b^* = \Phi^T \mathbf{K}_b \Phi$.

3. Numerical models

3.1 Train

Table 3 lists the train's natural frequencies, indicating that the fundamental frequencies related to bounce and sway are 1.207 Hz and 0.912 Hz, respectively.

3.2 Bridge

A modern bridge design requires not only strength but also cost-efficiency, and the situation stimulate structural engineers bring about a concept of rationalized design strategy even in monorail structures. New types of rationalized steel bridges for monorails thus have been developed. It also adopts the RC tramway to enhance braking performance.

The general layout and the basic geometry of the rationalized and conventional type bridges are presented in Fig. 4, whereas Fig. 5 shows those FE models. The rationalized bridge equipped less lateral members than conventional bridge to enhance the works regard to fabrication, erection, maintenance, and others. Table 4 compares the design of the rationalized bridge with the conventional one briefly. The bridge's span length is 42.8m. Table 5 shows the bridge's structural properties, in which: h indicates the girder height; t_w , t_{fu} and t_{fl} are the thickness of web, upper flange and lower flange, respectively; b_{fu} and b_{fl} indicate the respective widths of upper flange and lower flange; E represents Young's modulus; and σ_y shows the yield stress. The monorail car is assumed to travel along the G1 track girder (see Fig. 5) in this analysis.

First ten natural modes and related frequencies of the bridges are summarized in Table 6, as taken from eigen value analysis. That table shows that the first lateral bending mode is the first mode of the conventional and rationalized bridges with natural frequencies of 2.574Hz and 1.797Hz, respectively. The first vertical bending mode of bridges is 3.059Hz and 2.993Hz for conventional and rationalized bridges, respectively. The comparison of the natural frequencies in relation to the vertical and lateral bending modes of the bridges with those for bouncing and sway of a train indicates low possibility of resonance between two systems.

It is noteworthy that the rationalized bridge has a lower frequency in relation to lateral bending than that of a conventional bridge, meaning that the rationalized bridge is affected more easily by

lateral loading effects than the conventional bridge.

3.3 Surface roughness

Surface profiles of tracks for driving, steering, and stabilizing wheels are generated by means of a Monte-Carlo simulation method using a power spectral density (PSD) function [19] as shown in Eq. (15)

$$S_{z0}(\Omega) = \frac{\alpha}{\Omega^n + \beta^n}, \quad (15)$$

where $\Omega (= \omega/2\pi)$ is the space frequency; and α , β and n are the roughness coefficient, shape parameter, and a parameter to express the power distribution of a given PSD curve, respectively.

The parameters of Eq. (15) are assumed to follow data taken from a measurement on an existing monorail bridge with span of 36m long [12]. For information, Fig. 6 shows the surface profile taken from the simulation and measurement.

Driving track: $\alpha = 0.0005$, $\beta = 0.35$, $n = 3.00$

Track for steering wheel: $\alpha = 0.0006$, $\beta = 0.5$, $n = 2.80$

Track for stabilizing wheel: $\alpha = 0.0006$, $\beta = 0.5$, $n = 2.60$

Figure 7 shows PSD curves with the ISO estimate [20]. Although the Eq. (15) and the ISO estimate are for the roadway surface, the estimate is also adopted for the dynamic response analysis of the monorail bridges because of no available data for monorail bridges. The surface condition is categorized as roughness class 'A', corresponding to a very smooth condition according to ISO 8606 based on the vehicles' riding comfort. Such a road class typically indicates a newly paved highway. The PSD functions defining the eight road classes A to H according to the ISO 8606 code (1995) [20]. Paved roads are generally considered to be among roadway roughness classes A to D. An unpaved road where a truck could hardly travel at a speed of 40 km/h corresponds to surface roughness class E or F.

4. Dynamic responses of monorail bridges

Guyan reduction is used for the sake of computational effectiveness [18]. Acceleration responses of the bridge are estimated by superposing up to the 50th mode (conventional type bridge;

127.01Hz, rationalized type bridge; 100.41Hz) because preliminary analysis indicates that dynamic responses are sufficiently convergent within the 50th mode. Forty samples of the simulated surface profiles are considered. In analysis trains are assumed to running on surface roughness before entering the bridge to consider initial conditions of trains.

Newmark's β method [21] is adopted to solve simultaneous differential equations of the monorail bridge-train interaction system. The value of 0.25 is adopted for β to obtain stable and accurate solutions. The time interval is assumed to be shorter than 1/6 of the natural frequency of the highest mode in consideration. The solution can be obtained within the tolerance margin of 0.001.

4.1 Displacement responses of bridges

Figure 8 and Figure 9 show displacement responses at the span center in vertical and lateral directions (train speed 20m/s, no passenger), respectively. Regarding vertical responses, the static response of the rationalized bridge is smaller than that of the conventional bridge because of larger vertical bending stiffness of the rationalized bridge than that of the conventional bridge. There is little difference in the dynamic response. In contrast, the dynamic component of the rationalized bridge in the lateral direction becomes larger than that of the conventional bridge because of the simplified lateral bracing system, even though the static response of the rationalized bridge in the lateral direction is smaller than that of the conventional bridge.

It is noteworthy that the static response in the lateral direction shown in Fig. 9 results from the torsional effect arising from eccentricity between the bridge's shear center and the trains' vertical loads.

4.2. Dynamic response of the rationalized bridge

The simplified lateral bracing system of the rationalized bridge vibrates more easily than that of the conventional bridge, especially in the lateral direction as previously stated. Therefore, investigation on vibration of the rationalized bridge is required.

4.2.1 Effect of train speed

The dynamic component of the displacement response of the rationalized bridge is simulated as

shown in Fig. 10 with respect to train speeds of 36km/h (10m/s), 54km/h (15m/s), and 72km/h (20m/s) under the condition of no passenger to investigate the effect of train speed on dynamic response of the monorail bridge. Results show that lateral responses of the bridge tend to increase according to train speed.

4.2.2 Effect of passenger loading

Figure 11 shows the dynamic displacement response of the rationalized bridge with respect to passenger loading for traveling speed of 72km/h (20m/s) with no passenger (262.4kN), a normal operation condition (129 passengers, 338.3kN), and a fully loaded condition (270 passengers, 420.7kN). The amplitude of the bridge's dynamic response in a lateral direction apparently decreases according to passenger loading. Nevertheless, no clear changes are observed for dynamic response in the vertical direction.

5. Riding comfort of monorail train

Riding comfort of monorail train is investigated on the rationalized bridge because the dynamic lateral responses of the rationalized bridge are larger than those of the conventional bridge, as noted in section 4.

5.1 Effect of train speed

Dynamic acceleration responses and root mean square (RMS) values of vertical and lateral acceleration responses at the front bogie of the head car with respect to speed are shown in Fig. 12 and Fig.13, respectively. The vertical response and the RMS value of the train increase according to the train speed. However, the acceleration and its RMS value tend to decrease in the lateral direction with increasing speed.

5.2 Effect of passenger loading

Figure 14 shows acceleration responses at the head car's front bogie according to the number of passengers. Figure 15 summarizes effects of passenger loading on the acceleration response of the

car. For vertical and lateral vibrations, the largest RMS value is obtainable with no passengers.

5.3 1/3 octave band frequency analysis

Figure 16 shows 1/3 octave band spectra of the train's acceleration response compared with the fatigue-decreased proficiency boundary for the riding quality level of ISO 2631[13, 14]. This analysis uses the speed and passenger number which give the maximum RMS value for the most case. The limits for vertical and horizontal vibrations are expressed as a function of frequencies according to the exposure time from one minute to 24 hours. It is noteworthy that the most sensitive frequency ranges are 4 Hz to 8 Hz for the vertical vibration and below 2 Hz for the lateral vibration; hence, the dotted rectangle in Fig. 16 indicates the frequency range.

Riding comfort of monorail trains is estimated considering 40 surface roughness samples that are generated using Monte-Carlo Simulation. The mean and standard deviation values are used to assess the riding comfort of the monorail train: the solid line represents mean values; the dashed-dotted line indicates the summation of mean and standard deviation; and the dashed-double dotted line shows summation of mean and two times standard deviation. For the most sensitive frequency ranges, the vertical and lateral accelerations locate, respectively, below one hour and two hours of the exposure time boundary, even in the critical case such as the mean and two times standard deviation of accelerations on the floor of the rear bogie. Consequently, the riding comfort of the train can be categorized as good because the total operation time between terminals takes about 36 minutes. This demonstrates that the simplified structural system of the rationalized monorail bridge has little effect on train riding comfort.

6. Conclusions

Traffic-induced vibration analysis of a monorail bridge and train considering track-roughness was carried out to investigate the riding comfort of trains running on a rationalized steel bridge with a simplified structural system. Some important conclusions can be summarized as follows:

- (1) The occurrence of resonance in the vertical and lateral directions is very low between monorail trains and rationalized or conventional bridges.
- (2) The rationalized bridge has a lower frequency in relation to lateral bending than that of a conventional bridge because of rationalized bridges' simplified lateral bracing system.

Therefore the rationalized bridge is affected more easily by lateral loading effects than the conventional bridge. However the study demonstrates that the dynamic responses of the monorail bridges do not directly affect the response of the trains on the bridges.

- (3) Observations also show that the amplitude of the bridge dynamic response increases in the lateral direction concomitant with speed; it decreases according to passenger loading.
- (4) The riding comfort of the monorail train can be categorized as good by ISO2631, even in the case of adopting a simplified structural system: on the most sensitive frequency ranges, the vertical and lateral accelerations locate, respectively, below one hour and two hours of the exposure time boundary, even in the critical case such as the mean and two times standard deviation of accelerations. The resultant riding comfort of the train can therefore be categorized as good even for total operation time between terminals of about 36 minutes.

REFERENCES

- [1] Kawatani M, Kim CW, Lee CH, Kamizono T, Nishimura N. Traffic-induced vibration analysis of monorail bridge under earthquake. The 3rd International Conference on Advances in Structural Engineering & Mechanics (ASEM04) Seoul, Korea, September 2004.
- [2] Diana G, Cheli F. Dynamic interaction of railway systems with large bridge. *Vehicle System Dynamics* 1989;18:71-106.
- [3] Fryba L. Dynamics of railway bridges. 2nd ed., London: Thomas Telford, 1996.
- [4] Yau JD, Yang YB, Kuo SR. Impact response of high speed rail bridges and riding comfort of rail cars. *Engineering Structures* 1999;21:836-44.
- [5] Au FTK, Wang JJ, Cheung YK. Impact study of cable-stayed bridge under railway traffic using various models. *Journal of Sound and Vibration* 2001;240(3):447-65.
- [6] Lei X, Noda NA. Analyses of dynamic response of vehicle and track coupling system with random irregularity of track vertical profile. *Journal of Sound and Vibration* 2002;258(1):147-65.
- [7] Ju SH, Lin HT. Numerical investigation of a steel arch bridge and interaction with high-speed trains. *Engineering Structures* 2003;25:241-50.
- [8] Song MK, Noh HC, Choi CK. A new three-dimensional finite element analysis model of high-speed train-bridge interactions. *Engineering Structures* 2003;25:1611-26.
- [9] Kwark JW, Choi ES, Kim YJ, Kim BS, Kim SI. Dynamic behavior of two-span continuous concrete bridges under moving high-speed train. *Computers and Structures* 2004;82:463-74.
- [10] Hutton SG, Cheung YK. Dynamic response of single span highway bridges. *Earthquake Eng Struct Dyn*

1979;7:543-53.

- [11] Kawatani M, Kim CW. Computer simulation for dynamic wheel loads of heavy vehicles. *Journal of Structural Engineering and Mechanics*. 2001;12:409-28.
- [12] Lee CH, Kawatani M, Kim CW, Nishimura N, Kobayashi Y. Dynamic response of a monorail steel bridge under a moving train. *Journal of Sound and Vibration*. (submitted)
- [13] ISO2631/1. Evaluation of human exposure to whole-body vibration – Part 1: General requirements. 1985
- [14] ISO2631/2. Evaluation of human exposure to whole-body vibration – Part 2: Continuous and shock-Induced vibration in buildings (1 to 80Hz). 1989.
- [15] Hurty WC, Rubinstein MF. *Dynamics of structures*. Englewood Cliffs, NJ: Prentice-Hall 1960;90-103.
- [16] Thomson WT. *Theory of Vibration with Applications*. Englewood Cliffs, NJ: Prentice-Hall 1988;196-198.
- [17] Agabain ME. The effect of various damping assumptions on the dynamic response of structures. *Bulletin of International Institute of Seismology and Earthquake Engineering* 1971;8:217-36.
- [18] Guyan RJ. Reduction of stiffness and mass matrices. *AIAA J* 1965;3(2):380.
- [19] Honda H, Kajikawa Y, Kobori T. Spectra of road surface roughness. *ASCE Structural Division* 108(ST9) 1982;1956-66.
- [20] ISO 8606. *Mechanical Vibration – Road Surface Profiles - Reporting of Measured Data*. ISO, 1995.
- [21] Newmark NM. A Method of computation for structural dynamics. *ASCE J of Eng Mech Div* 1970;96:593-620.

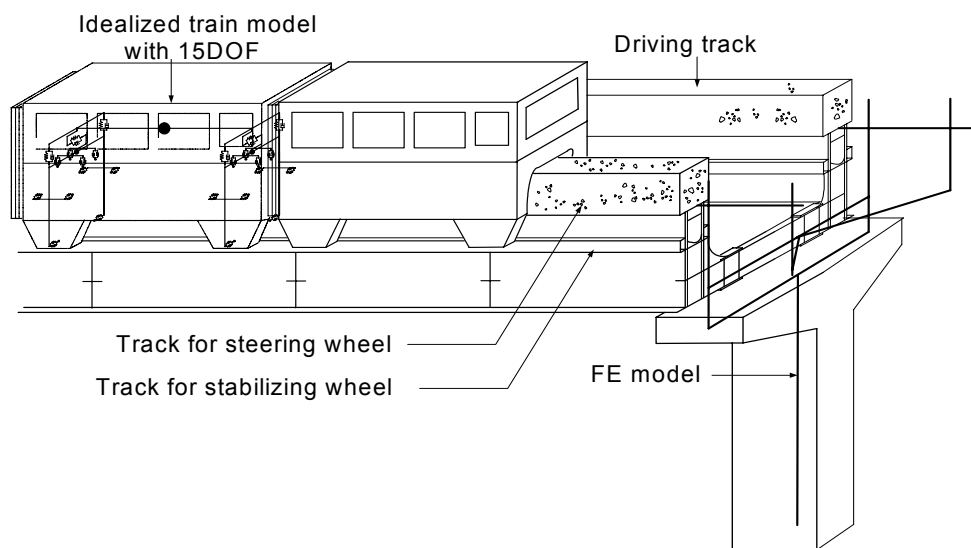


Fig. 1 Scheme for a monorail bridge-train interaction system

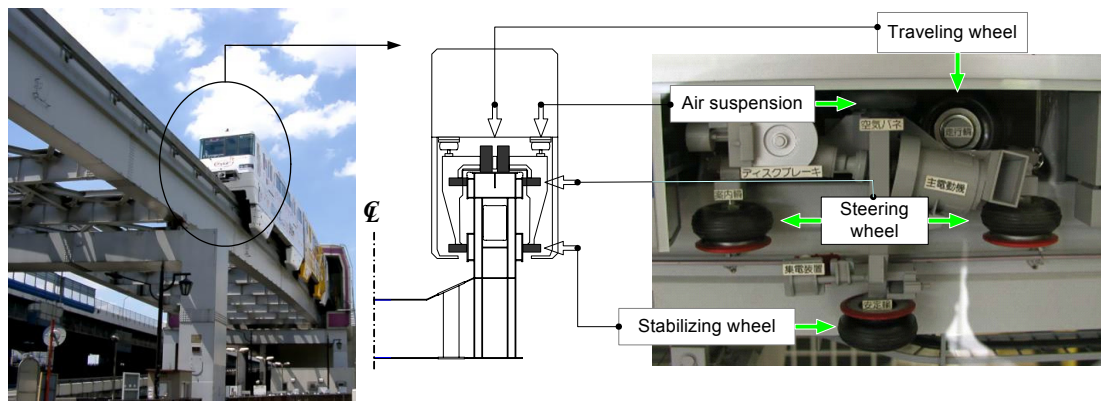


Fig. 2 Configuration of straddle-type monorail train on a track girder

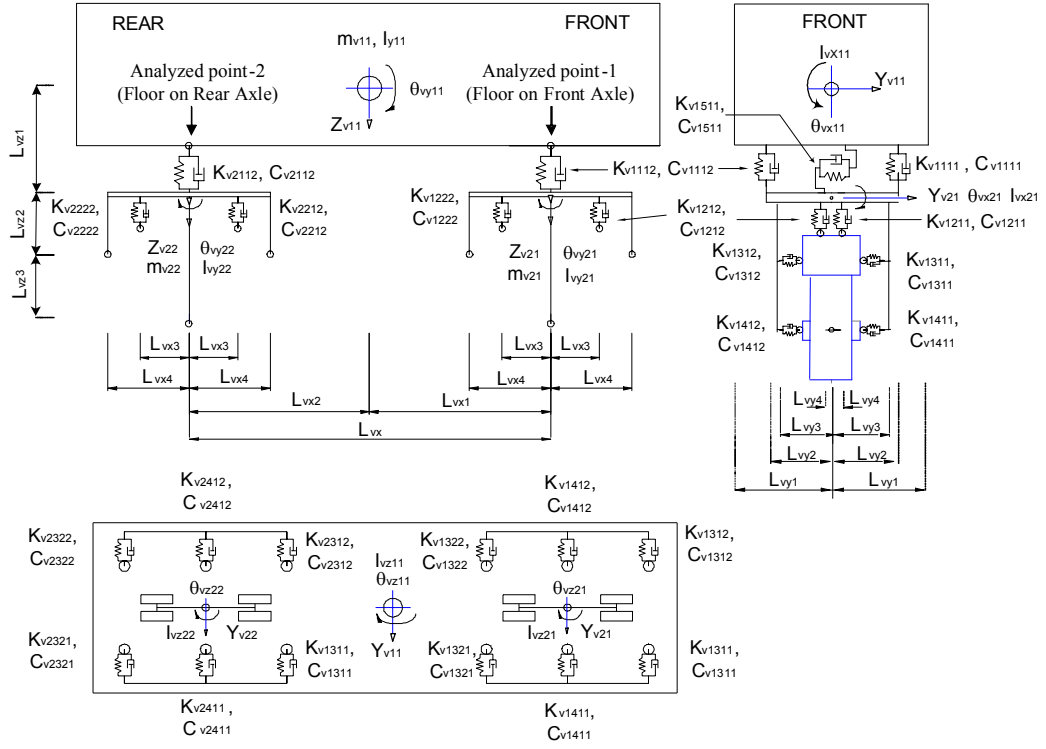


Fig. 3 Idealized monorail train with 15DOF

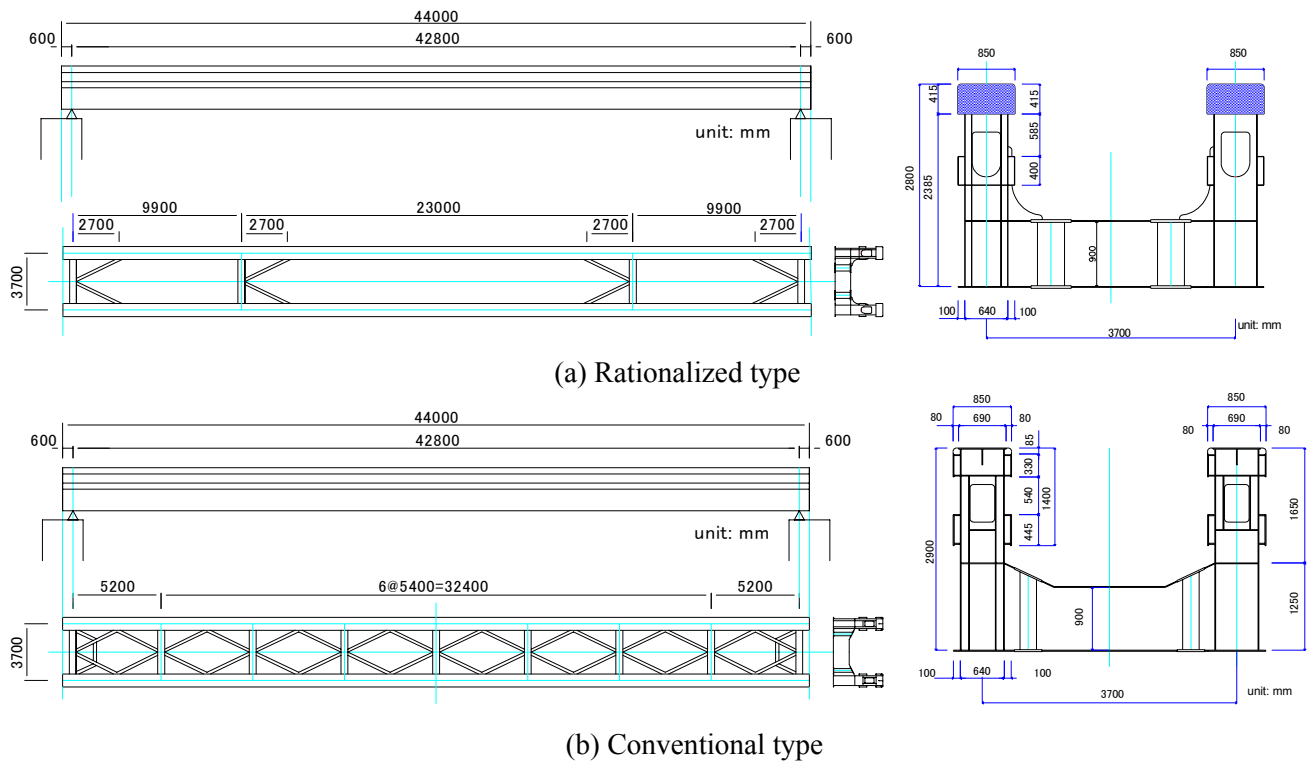


Fig. 4 General layout of monorail bridges

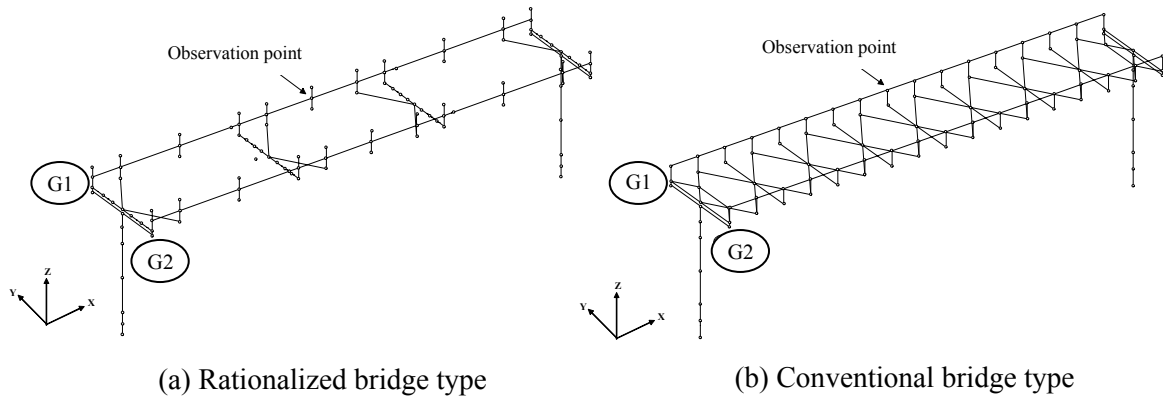


Fig. 5 FE models

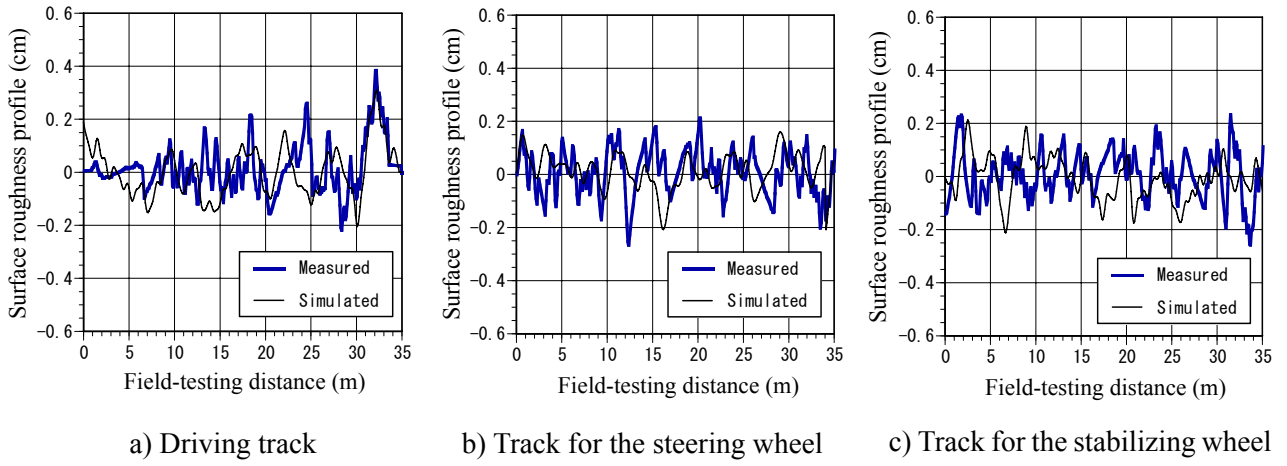


Fig. 6 Comparison of simulated surface roughness with measured data

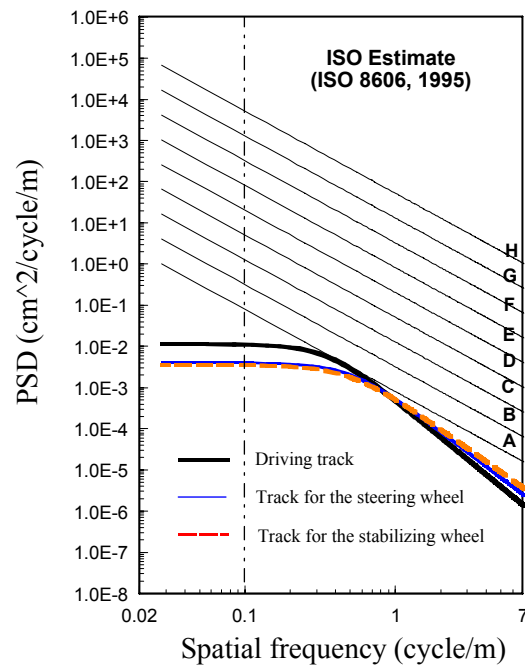
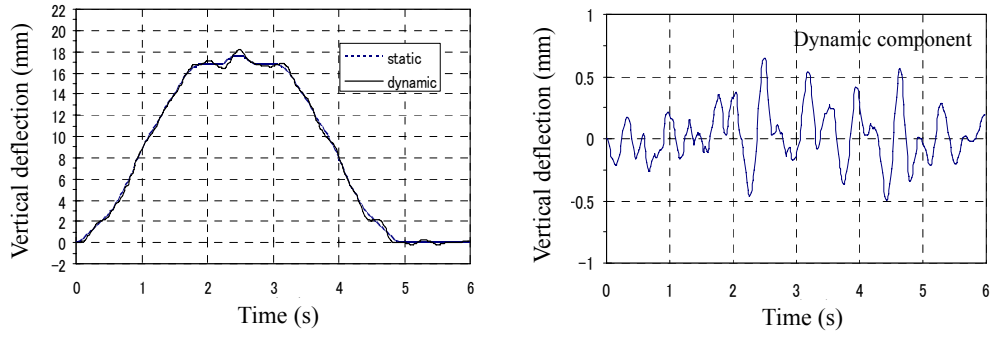
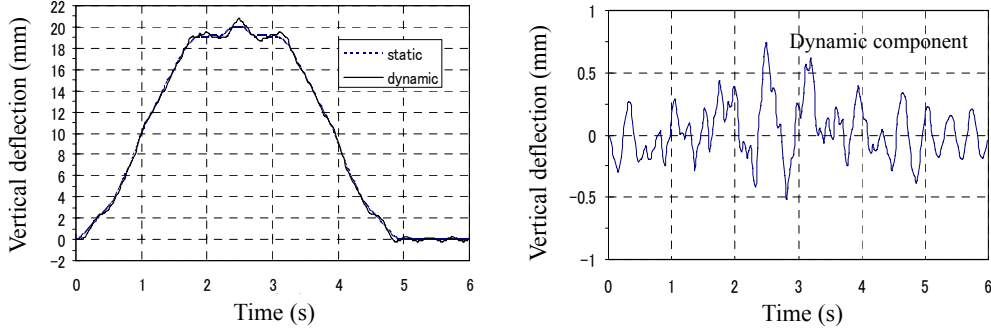


Fig. 7 PSD curve of surface roughness (A~D: Paved roads; E~F: Unpaved road where a truck could hardly travel at a speed of 40 km/h)

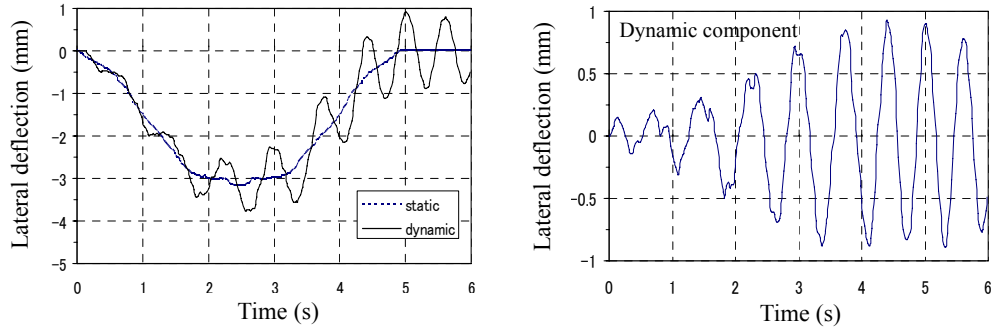


(a) Rationalized bridge

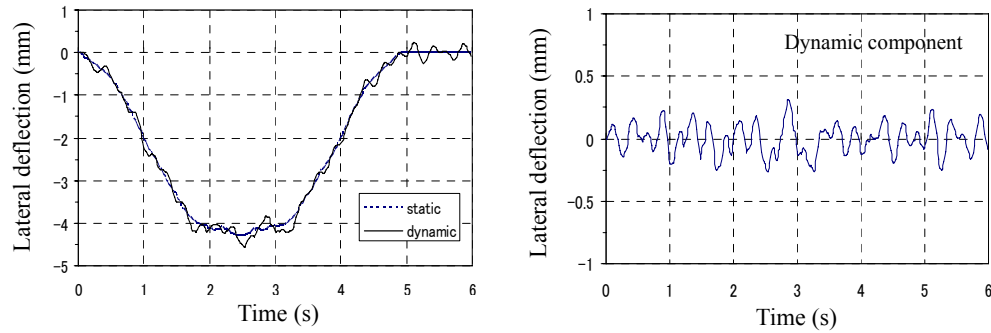


(b) Conventional bridge

Fig. 8 Vertical response at the center of span (no passenger, $v=20\text{m/s}$)



(a) Rationalized bridge



(b) Conventional bridge

Fig. 9 Lateral response at the center of span (no passenger, $v=20\text{m/s}$)

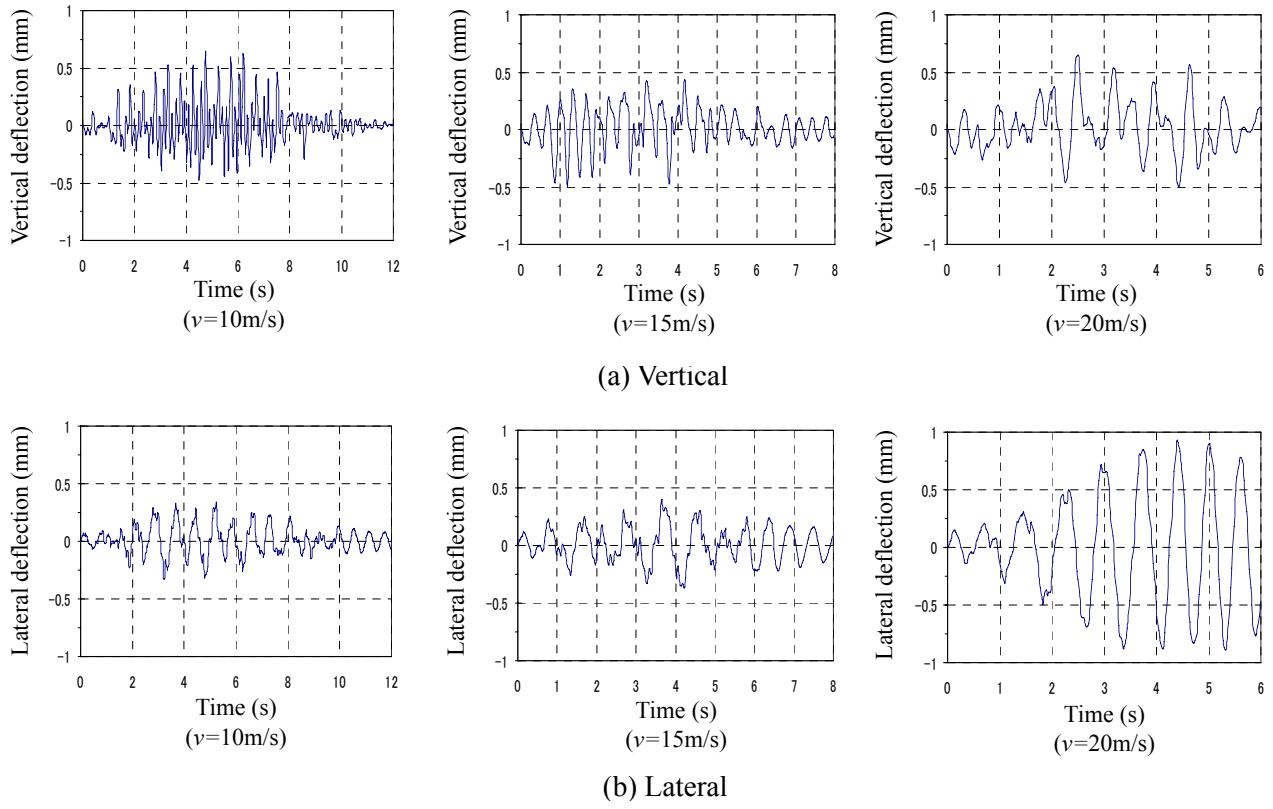


Fig. 10 Dynamic responses at the center of span according to car speeds (No passenger)

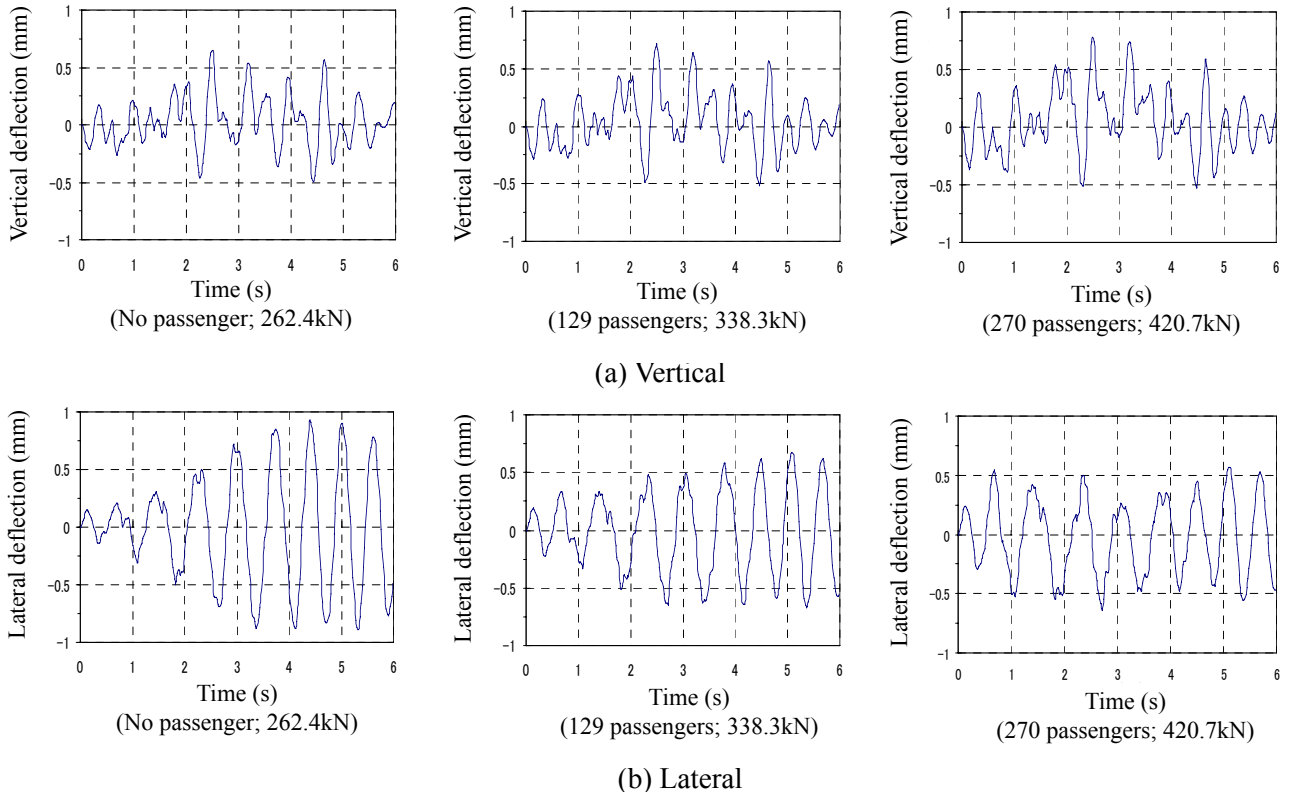
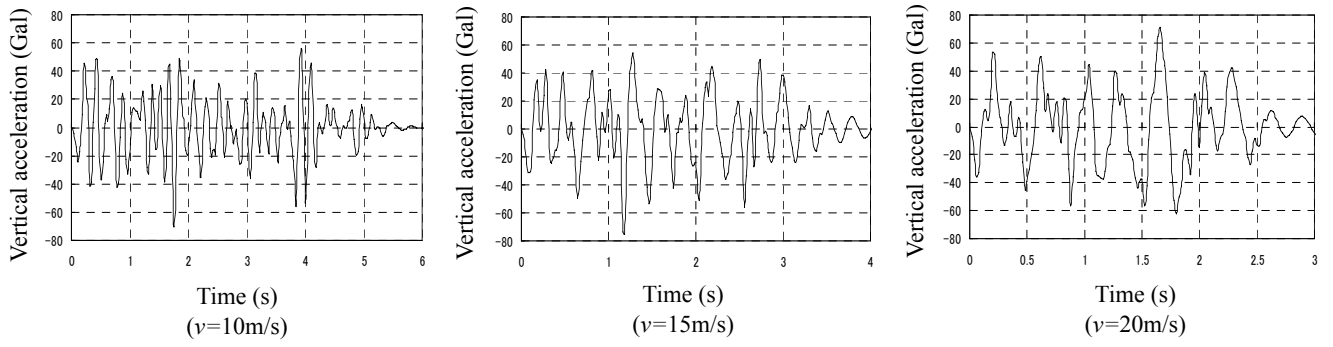
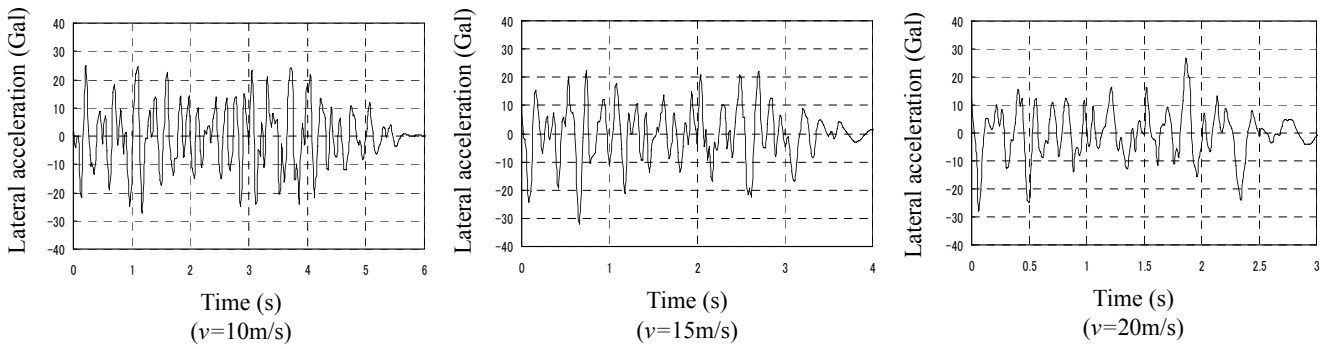


Fig. 11 Dynamic responses at the center of span according to passenger loading ($v=20\text{m/s}$)

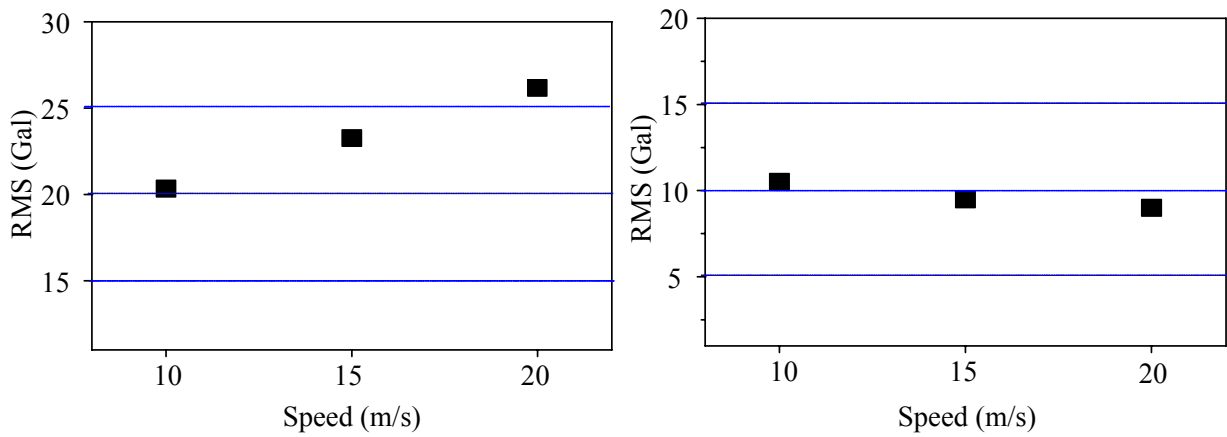


(a) Vertical



(b) Lateral

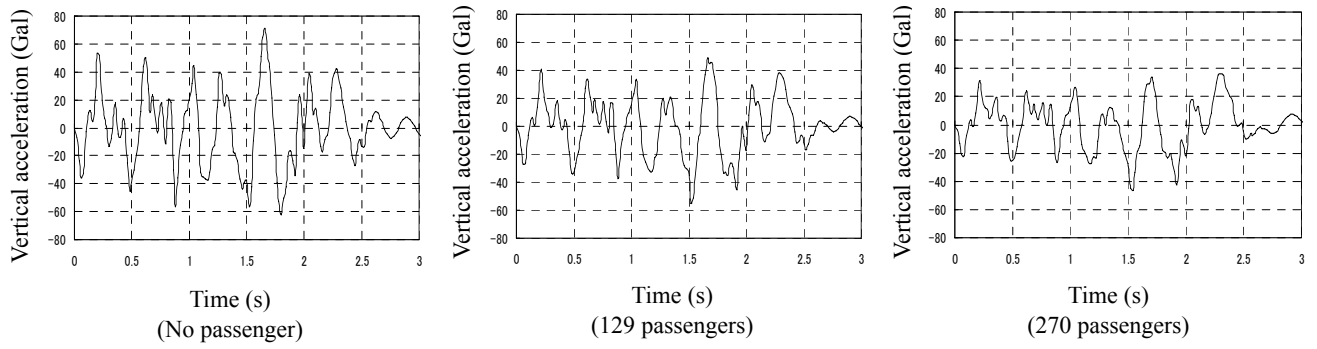
Fig. 12 Dynamic responses at the front bogie of the head car according to speed (No passenger)



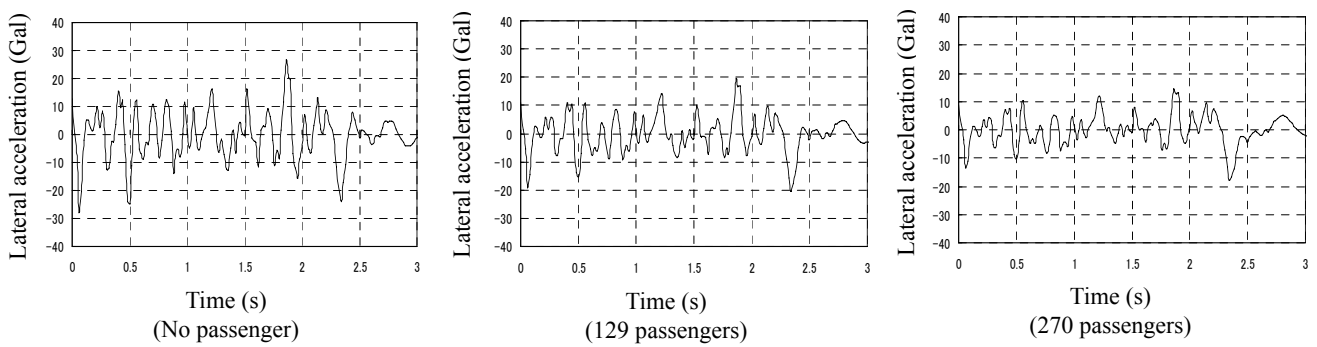
(a) Vertical

(b) Lateral

Fig. 13 Effect of running speed for the monorail train (No passenger)

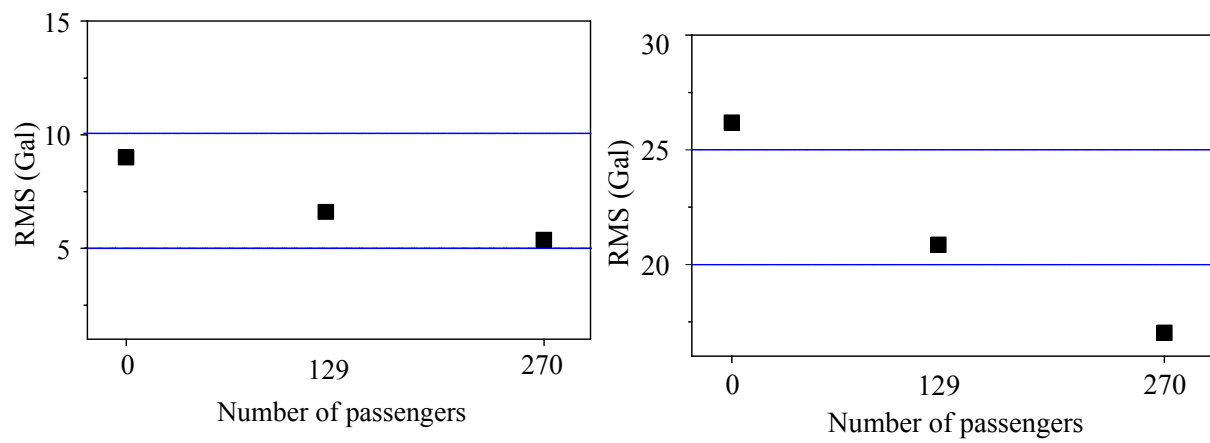


(a) Vertical



(b) Lateral

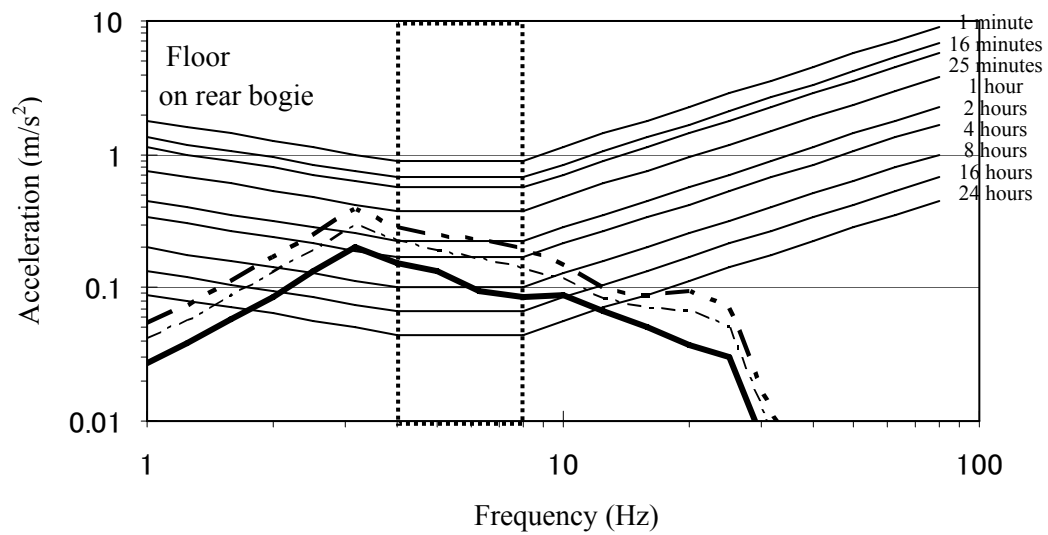
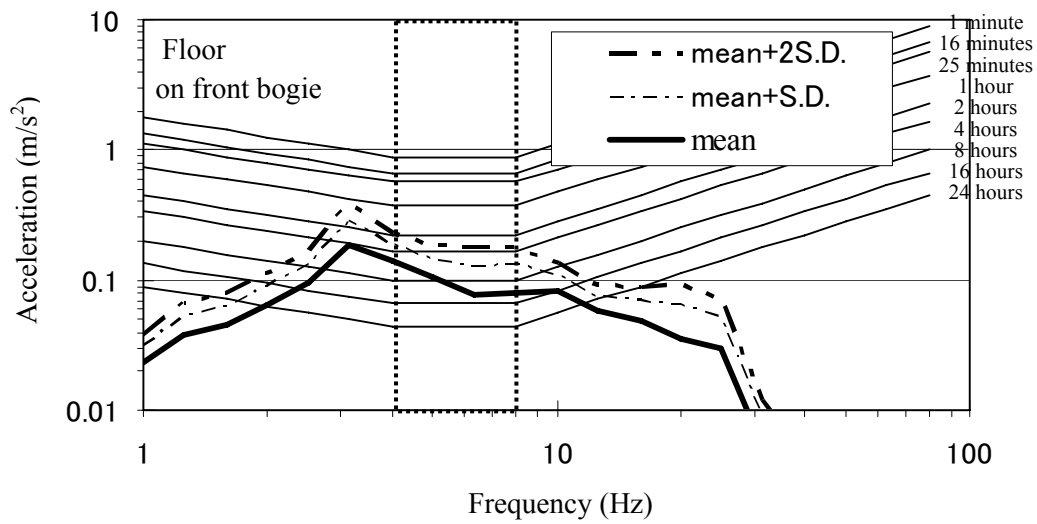
Fig. 14 Dynamic responses at the front bogie of the head car according to passenger loading ($v=20\text{m/s}$)



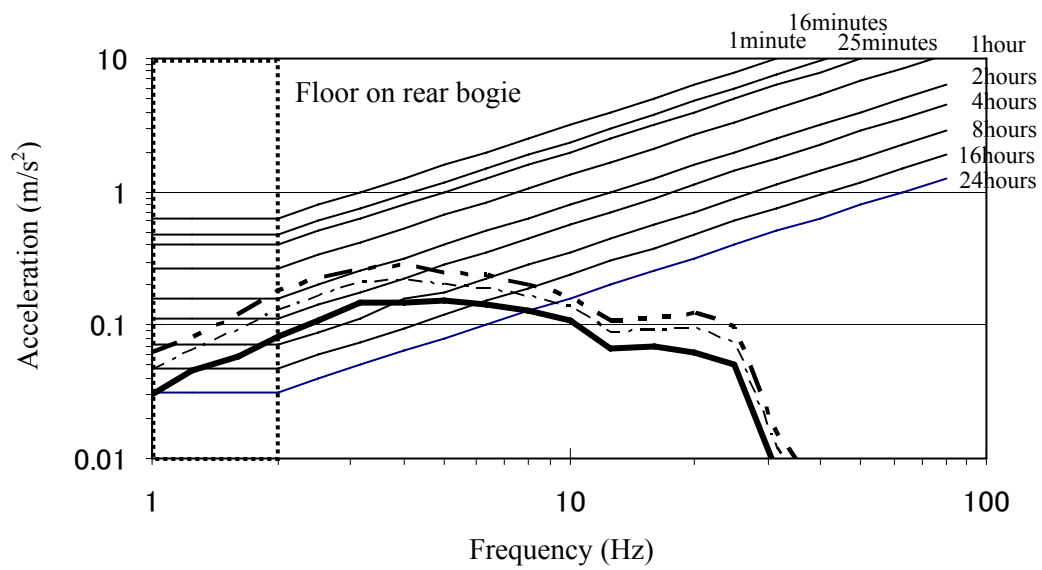
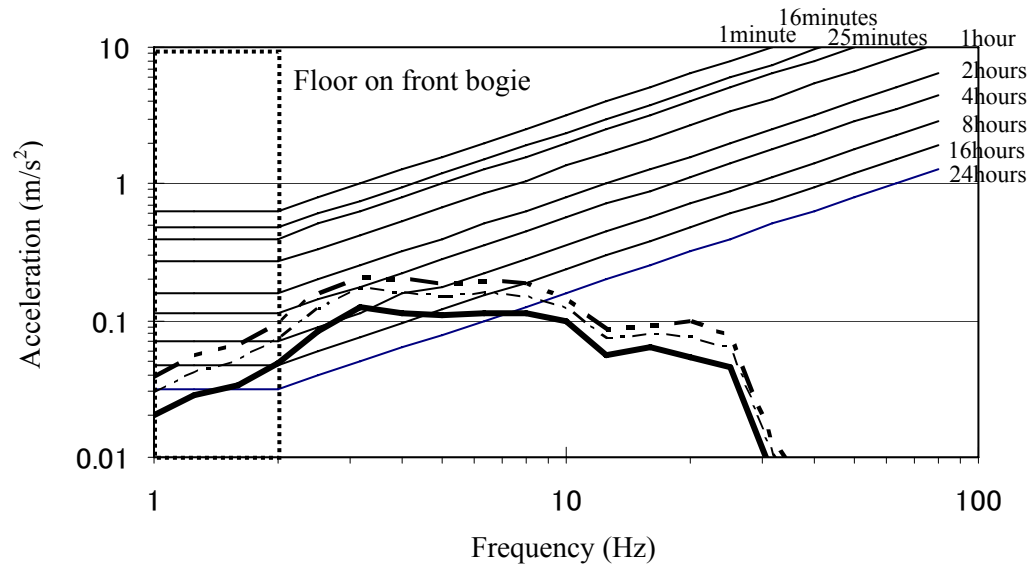
(a) Vertical

(b) Lateral

Fig. 15 Effect of passenger loading condition for the monorail train ($v=20\text{m/s}$)



(a) Vertical



(b) Lateral

Fig. 16 Riding comfort of a monorail train: ISO2631 ($v=20\text{m/s}$, no passenger)

Table 1 Train model notation

Description	Notation
Mass of body	m_{v11}
Mass of suspension system	m_{v21}, m_{v22}
Spring constant of air suspension (Vertical)	$K_{v1111}, K_{v1112}, K_{v2111}, K_{v2112}$
Spring constant of driving wheel	$K_{v1211}, K_{v1212}, K_{v1221}, K_{v1222}$ $K_{v2211}, K_{v2212}, K_{v2221}, K_{v2222}$
Spring constant of steering wheel	$K_{v1311}, K_{v1312}, K_{v1321}, K_{v1322}$ $K_{v2311}, K_{v2312}, K_{v2321}, K_{v2322}$
Spring constant of stabilizing wheel	$K_{v1411}, K_{v1412}, K_{v2411}, K_{v2412}$
Spring constant of air suspension (Lateral)	K_{v1511}, K_{v2511}
Damping constant of damper (Vertical)	$C_{v1111}, C_{v1112}, C_{v2111}, C_{v2112}$
Damping constant of driving wheel	$C_{v1211}, C_{v1212}, C_{v1221}, C_{v1222}$ $C_{v2211}, C_{v2212}, C_{v2221}, C_{v2222}$
Damping constant of steering wheel	$C_{v1311}, C_{v1312}, C_{v1321}, C_{v1322}$ $C_{v2311}, C_{v2312}, C_{v2321}, C_{v2322}$
Damping constant of stabilizing wheel	$C_{v1411}, C_{v1412}, C_{v2411}, C_{v2412}$
Damping constant of damper (Lateral)	C_{v1511}, C_{v2511}
Vertical and lateral body displacements	Z_{v11}, Y_{v11}
Vertical displacements of front and rear suspension system	Z_{v21}, Z_{v22}
Lateral displacements of front and rear suspension system	Y_{v21}, Y_{v22}
Rolling, pitching and yawing of body	$\theta_{vx11}, \theta_{vy11}, \theta_{vz11}$
Rolling of front and rear suspension system	$\theta_{vx21}, \theta_{vx22}$
Pitching of front and rear suspension system	$\theta_{vy21}, \theta_{vy22}$
Yawing of front and rear suspension system	$\theta_{vz21}, \theta_{vz22}$

Table 2 Properties of a monorail train

Body		Bogie		Geometry	
m_{v11}	14.22×10^3 (kg)	m_{v21}, m_{v22}	6.20×10^3 (kg)	L_{vx1}, L_{vx2}	4.800 (m)
I_{vx11}	1.997×10^4 (kg·m ²)	I_{vx21}, I_{vx22}	2.461×10^3 (kg·m ²)	L_{vx3}	0.7500 (m)
I_{vy11}	1.717×10^5 (kg·m ²)	I_{vy21}, I_{vy22}	3.488×10^3 (kg·m ²)	L_{vx4}	1.250 (m)
I_{vz11}	1.717×10^5 (kg·m ²)	I_{vz21}, I_{vz22}	9.688×10^3 (kg·m ²)	L_{vy1}	1.490 (m)
K_{vz11}	9.0×10^5 (N/m)	K_{vz21}, K_{vz22}	5.170×10^6 (N/m)	L_{vy2}	1.025 (m)
K_{vy11}	9.80×10^5 (N/m)	K_{vy21}, K_{vy22}	6.370×10^6 (N/m)	L_{vy3}	0.7823 (m)
C_{vz11}	2.28×10^4 (N·s/m)	C_{vz21}, C_{vz22}	2.610×10^4 (N·s/m)	L_{vy4}	0.200 (m)
C_{vy11}	3.336×10^5 (N·s/m)	C_{vy21}, C_{vy22}	1.855×10^5 (N·s/m)	L_{vz1}	0.885 (m)
				L_{vz2}	0.6300 (m)
				L_{vz3}	1.085 (m)

Table 3 Natural frequencies of a vehicle (no passenger)

Mode	Frequency (Hz)
Bouncing: f_{z11}	1.207
Axle hop (Front) : f_{z21}	5.960
Axle hop (Rear) : f_{z22}	5.960
Sway: f_{y11}	0.912
Bogie sway (Front) : f_{y21}	4.090
Bogie sway (Rear) : f_{y22}	4.090
Rolling: $f_{\theta x11}$	1.660
Axle tramp (Front) : $f_{\theta x21}$	4.616
Axle tramp (Rear) : $f_{\theta x22}$	4.616
Pitching: $f_{\theta y11}$	1.790
Bogie windup (Front) : $f_{\theta y21}$	4.394
Bogie windup (Rear) : $f_{\theta y22}$	4.394
Yawing of a body: $f_{\theta z11}$	2.286
Yawing of a front bogie : $f_{\theta z21}$	4.003
Yawing of a rear bogie : $f_{\theta z22}$	4.003

Table 4 Comparison of rationalized and conventional monorail bridges


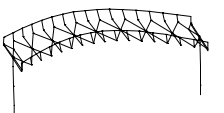

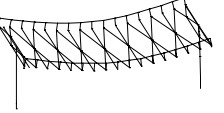

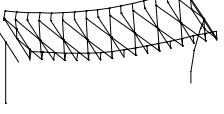


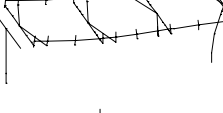

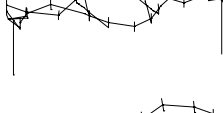






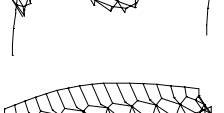
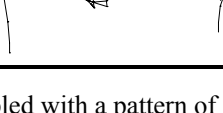
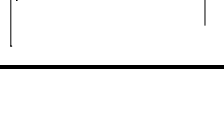
Items	Conventional type bridge	Rationalized type bridge
Main girder	Steel-slab	RC-slab
Floor system of driving track Track for the stabilizing wheel	Steel plate + strengthening rib	Mold steel + grouting mortar
Cross beam (CB)	Consists of nine CB's	Consists of four CB's
Lateral bracing (LB)	Consists of 38 LB's	Consists of eight LB's
Weight*	715 kN / span	980 kN / span

* L=44m

Table 5 Properties of monorail bridges

Items	h (mm)	t_w (mm)	b_{fu} (mm)	t_{fu} (mm)	b_{fl} (mm)	t_{fl} (mm)	E (GPa)	ν	σ_y (MPa)
Rationalized bridge									
Main steel girder	2385	11	640	13	640	25	205	0.3	353
Concrete slab	415		850				45	0.167	45
End of cross beam	844	16	300	28	300	28	205	0.3	235
Center of cross beam	652	13	300	24	300	24	205	0.3	235
Lateral bracing	176	8	200	12	200	12	205	0.3	235
Conventional bridge									
Main steel girder	2781	11	690	18	860	19	205	0.3	353
End of cross beam	678	11	400	22	400	22	205	0.3	235
Center of cross beam	681	9	320	19	320	19	205	0.3	235
Lateral bracing	134	12	0	0	204	10	205	0.3	235

Table 6 First ten natural modes of bridge models

Rationalized bridge			Conventional bridge	
Mode No.	Mode	Frequency	Mode	Frequency
1		Lateral bending 1st/T1 1.797Hz		Lateral bending 1st/T1 2.574Hz
2		Vertical bending 1st 2.993Hz		Vertical bending 1st 3.059Hz
3		Lateral bending 2nd/T1 4.883Hz		Pier 1st (C/W vertical bending) 4.252Hz
4		Torsion 1st/T1 5.361Hz		Lateral bending 2nd/T1 6.322Hz
5		Pier 1st (C/W vertical bending) 6.129Hz		Torsion 1st/T1 (C/W Pier) 8.956Hz
6		Lateral bending 1st/T2 7.455Hz		Torsion 1st/T2 9.618Hz
7		Lateral bending 2nd/T2 8.730Hz		Lateral bending /T1 (C/W; Pier) 10.966Hz
8		Torsion 1st/T2 9.252Hz		Vertical bending 2nd (C/W horizontal bending) 12.466Hz
9		Lateral bending 3rd/T1 9.444Hz		Lateral bending 3rd/T1 (C/W horizontal bending) 15.462Hz
10		Lateral bending 2nd/T1 (C/W Pier) 10.259Hz		Torsion 2nd/T2 18.752Hz

* C/W: coupled with a pattern of a related mode

** T1: both track girders have similar phase; T2: both track girders have the reverse phase